Chapter 3

Life Prediction of Low Cycle Fatigue Behavior of Rotating Cantilever Beam of aluminium alloy AA6063-T6 at Room Temperature

3.1 Introduction

In this chapter low cycle fatigue analysis of AA6063 alloy is presented theoretically and experimentally for circular cross section subjected to monotonic and cyclic elastic–plastic pure bending. The rotating bending approach is adopted for determination of low-cycle fatigue parameters. The stress ratio of R = -1 is induced on the circular cross-section cantilever specimen loaded with a pure bending moment, and exposed to the rotation with respect of its longitudinal axis. The cyclic strain–stress response and strain life fatigue curves are plotted. The cyclic strain hardening exponent, cyclic strength coefficient, fatigue strength exponent and fatigue ductility exponent were found to be almost constant, being 0.14583, 618.75 MPa, -0.105 and -0.72 respectively. It is found that theoretical values of $n^{'}$ and $K^{'}$ are in good agreement to that obtained experimentally.

3.2 Results

Chemical composition results of as received AA6063 aluminium alloy sample by chemical analysis method and EDAX method are shown in Table 3.1. Chemical composition analysis by two methods provide good agreement.

The elemental distribution mapping of EDAX for the sample of AA6063 is illustrated in Fig. 3.1. The EDAX spectrum shows the presence of various elements in the

Life Prediction of Low Cycle Fatigue Behavior of Rotating Cantilever Beam of aluminium alloy AA6063-T6 at Room Temperature

Chapter 3

AA6063 surface. The spectra show a considerable increase in aluminum content, suggesting that the alloy should be a combination of aluminum alloy.

Table 3.1 Chemical composition and EDAX analysis for as-received AA6063-T6 alloy at room temperature

Element Weight%	Chemical Analysis	EDAX Analysis
AL Balance	99.17	88.60
Si	0.612	1.38
Mg	0.0798	0.82
Fe	0.0280	0.98
Cu	0.0374	0.64
Zn	0.0019	0.63
Mn	0.0132	0.51
Ti	0.0024	0.49
Cl	--	0.36
Ga	0.0197	--
S	0.0193	--
Ho	0.0070	--
Pb	0.0019	--
O	--	5.60
Error	0.83	0.26

The distribution of element concentration for line scanning of SEM/EDAX, indicates the analyzing area of the specific elements. It can be observed that the aluminum (Al) is the base and the Silicon (Si) and Magnesium (Mg) is first and second element present, respectively. The line scanning could investigate the variation of amounts of both elements that get into the other medium. On the other hand, the variation of element intensity also depicts the type of interfacial layer.
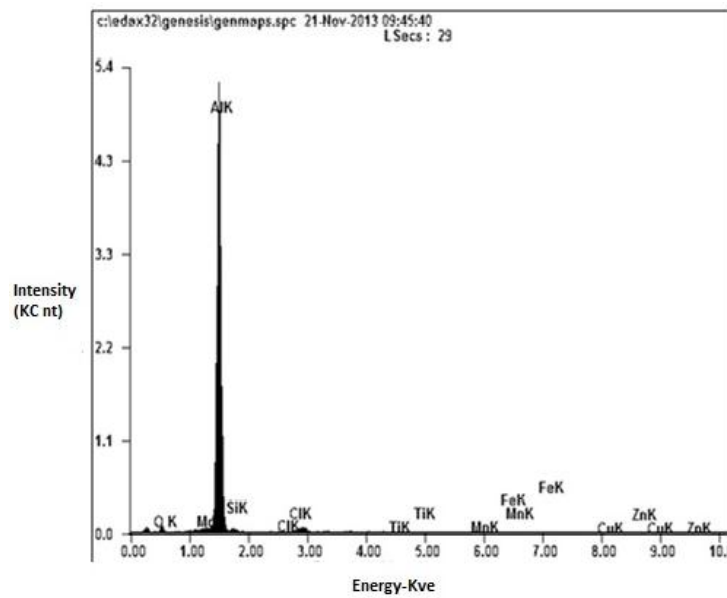
Life Prediction of Low Cycle Fatigue Behavior of Rotating Cantilever Beam of aluminium alloy AA6063-T6 at Room Temperature

Chapter 3

Fig. 3.1 EDAX spectrum of the AA6063-T6 alloy

Tensile test is performed before low cycle fatigue testing. Figure 3.2 illustrates the monotonic stress-strain results for as received AA6063 samples. It shows engineering, true and cyclic stress-strain curves for as received AA6063 samples.
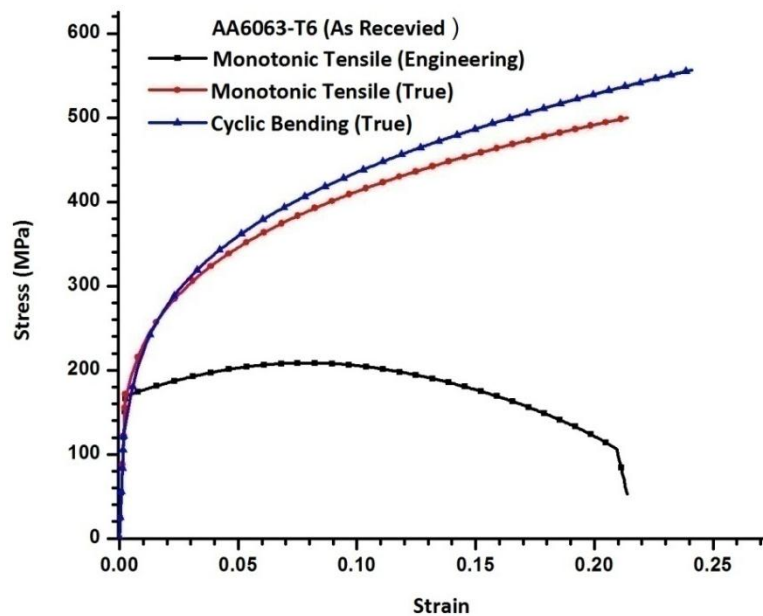

Fig. 3.2 Stress - Strain Curves for as received AA6063-T6 alloy

Life Prediction of Low Cycle Fatigue Behavior of Rotating Cantilever Beam of aluminium alloy AA6063-T6 at Room Temperature

Chapter 3

The SEM picture of the tensile sample after fracture is shown in Fig. 3.3. The figure clearly shows overload zone and decreasing cross-section and fracture zone. True plastic stress verses true plastic strain is plotted in log-log scale and a straight line approximation is obtained, as shown in Fig. 3.4. Strain hardness exponent (***n***) and strength coefficient (***K***) are calculated from this plot. Table 3.2 shows all the parameters obtained from monotonic tensile test.

Table 3.3 shows comparison of values of n, k and $\sigma_{fracture}^{true}$ obtained experimentally to that obtained by empirical relations given by Eqs. (2.68) to (2.70).
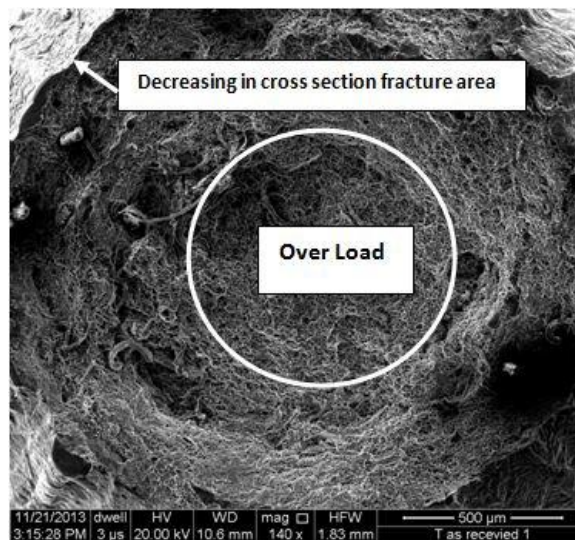
Fig. 3.3 Tensile fracture surface

Torsion test is also performed before low cycle fatigue test. Figure 3.5 shows shear stress versus shear strain diagram obtained from torsion test. The parameters obtained in torsion test are presented in Table 3.4 . The optical micrograph of torsion tested specimen shows the longitudinal grain shape due to the twist that happen in the test as shown in **Error! Reference source not found.**.
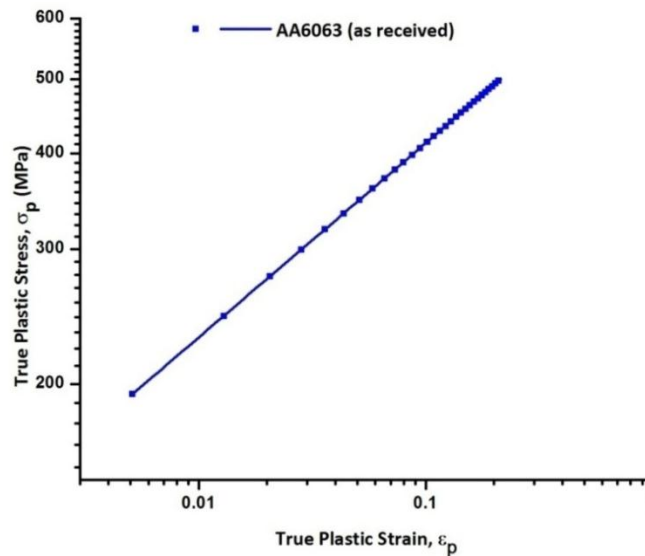
Fig. 3.4 Log-Log plot of true plastic stress versus true plastic strain

Table 3.2 Tensile properties for as-received AA6063-T6 alloy at room temperature

Parameter	Symbol	Value From graph	Value from equation (2.68)	Value from equation (2.69)	Value from equation (2.70)
Yield stress	σ_{YD}	169.67 MPa	--	--	--
Engineering Max. tensile stress	$\sigma_{Max.}$	214.8 MPa	--	--	--
Engineering Fracture strength	σ_f^{Eng}	54.2 MPa	--	--	--
Yield strain	ε_{YD}	0.002457	--	--	--
Young's modulus	E	68 GPa	--	--	--
% Strain at failure	ε_f	0.242	--	--	--
Toughness	K_C	m 41.417^3/J	--	--	--
Strain hardness exponent	n	0.25	0.25027	0.24988	0.25338
Strength coefficient	K	776.2MPa	776.2MPa	776.2 MPa	819.33Mpa

Table 3.3 Comparison of values of n, K and $\sigma_{fracture}^{true}$

Parameter	Experimental	Theoretical		
		Eq. (2.68)	Eq. (2.69)	Eq. (2.70)
n	0.25	0.25027	0.24988	0.25338
K	776.2	776.2	776.2	819.33
$\sigma_{fracture}^{true}$	237.49	527.56	666.29	499.82

Error! Reference source not found. and **Error! Reference source not found.**elaborate micro hardness and macro hardness test results respectively. Figure 3.7 shows variation of Vickers hardness values with different loads.

After performing tensile, torsion and hardness testing, low cycle fatigue testing was performed. Total of 21 samples were used. The cyclic data have been collected and given in Table 3.5. All data points are plotted in strain amplitude ($\frac{\Delta\varepsilon}{2}$) and number of cycles of failure ($2N_f$) plot as shown in Fig. 3.5. This is a log-log plot. Elastic strain data points are fitted in a straight line and plastic strain data points are fitted in a straight line. The intersection between these two lines is the transition fatigue life ($2N_T$) and the true stress amplitude at that life is denoted by $\frac{\Delta\sigma_S}{2}$. This point divides the whole plot into two regions viz. region I known as elastic region and region II known as plastic region. The total strain amplitude points are fitted as a curve (by least square method)which is asymptote to both elastic line and plastic line. Experimental fatigue parameters $\acute{n}$ and $\acute{k}$ of the aluminum alloy are found out from the strain –life curve, and Eqs. (2.5) and (2.6).

Table 3.4 Torsion test data for as-received AA6063-T6 alloy at room temperature

Parameters	symbol	Value
Max. shear strain (Deg)	$\gamma_{Max.}$	6.4
Max. angle of twist (Deg)	$\alpha_{Max.}$	100
Shear modulus (GPa)	**G**	25.9
Toughness (J/m³)	$K_{Max.}$	914
Max. shear stress (MPa)	$\tau_{Max.}$	209.03

Life Prediction of Low Cycle Fatigue Behavior of Rotating Cantilever Beam of aluminium alloy AA6063-T6 at Room Temperature

Chapter 3

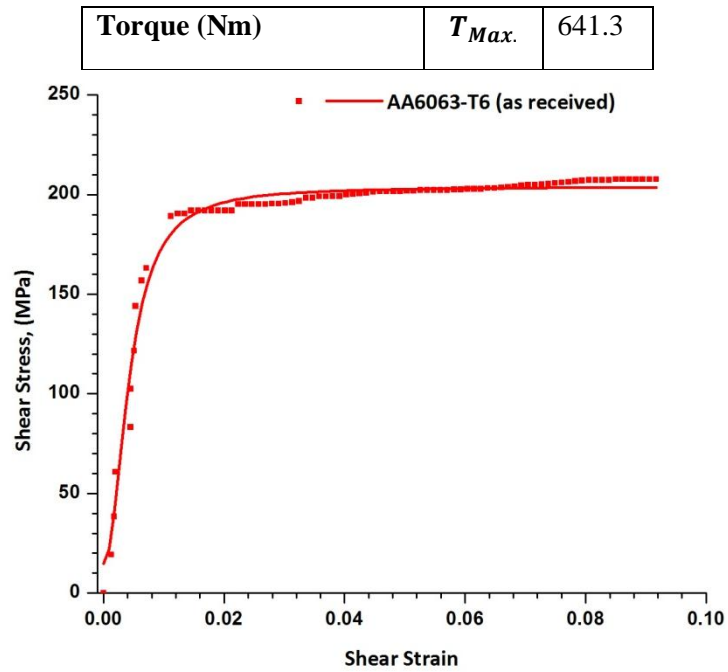| Torque (Nm)	$T_{Max.}$	641.3

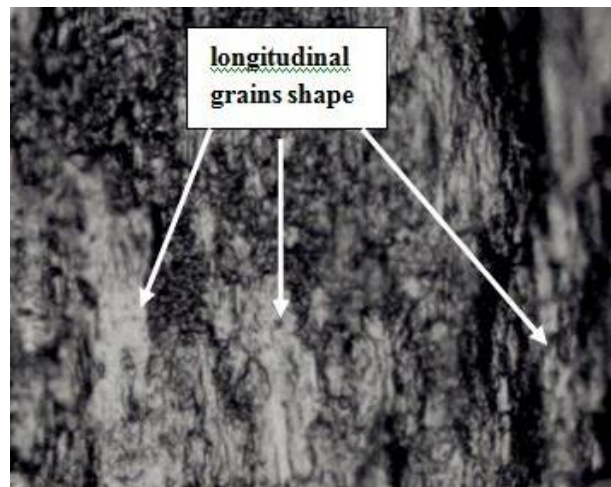**Fig. 3.5 Torsion test plot**

Fig. 3.6 Torsion tested fracture surface

Table 3.5 Vickers micro hardness for As Received AA6063-T6 alloy at different load

Load applied (kg)	HV
0.05	99.7875
0.09	100.575

Life Prediction of Low Cycle Fatigue Behavior of Rotating Cantilever Beam of aluminium alloy AA6063-T6 at Room Temperature

Chapter 3

0.19	100.725

Table 3. 6 Vickers Macro hardness for As Received AA6063-T6 alloy at different load

Load applied (kg)	HV
1	46.076
2	43.07
3	44.36
5	19.2
10	13.3
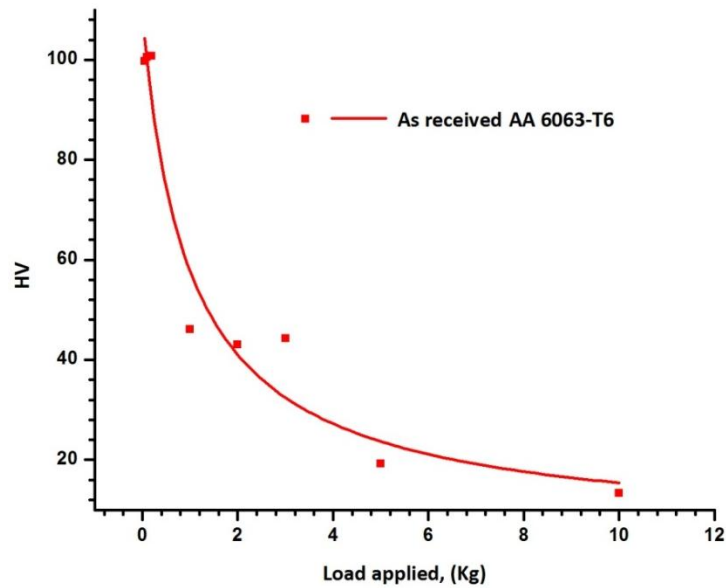
Fig. 3.7 Variation of Vickers hardness value for As Received AA6063-T6 alloy with different load

Table 3.5 Cyclic data for cantilever beam fatigue test of as-received AA6063-T6 at room temperature

| Number of cycles to failure (N_f)	Elastic Strain Amplitude	Plastic Strain Amplitude	Total Strain Amplitude
43560	0.00161	0	0.00161
63300	0.000965	0	0.000965
60150	0.00155	0	0.00155
15990	0.00206	0	0.00206
9750	0.0021	0	0.0021
7080	0.0029	0	0.0029
6690	0.0025	0	0.0025
3000	0.0035	0.00055	0.00405
444	0.0026	0.00501	0.00761
380	0.00269	0.00537	0.00806
350	0.00293	0.00585	0.00878
280	0.00343	0.00818	0.01161
200	0.00372	0.0123	0.01502
176	0.00404	0.01476	0.0198
133	0.00434	0.02077	0.02511
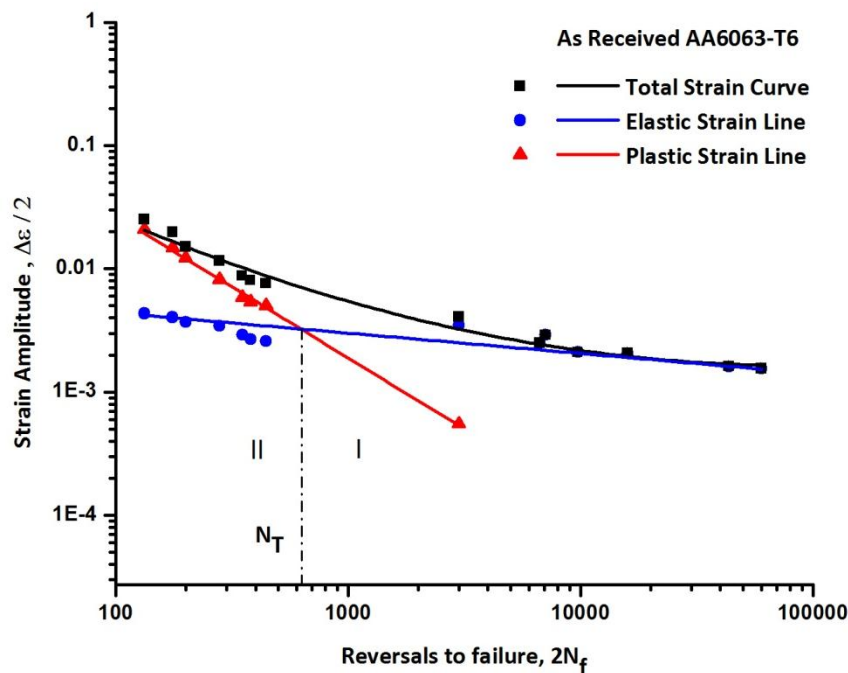
Fig. 3.5 Strain life curve for as-received AA6063-T6 alloy at room temperature

Table 3.6 Strain-controlled fatigue properties of as received AA6063-T6 aluminum alloy

Alloy	Cyclic plastic strain (Fatigue Ductility coefficient) ε_f'	Cyclic elastic strain σ_f'/E	Fatigue Strength Coefficient σ_f' (MPa)	fatigue strength exponent b	fatigue ductility exponent c	cyclic strain hardening exponent n´	cyclic strength coefficient K´ (MPa)	transition fatigue life N_T (cycles)
AA6063-T6	0.2915	0.006727	457.4	-0.165	-1.152	0.14322	545.7	632

The experimental LCF parameters viz. fatigue strength coefficient (σ_f') fatigue strength exponent (*b*), fatigue ductility coefficient (ε_f') and fatigue ductility exponent (*c*), cyclic strain hardening exponent n´ and cyclic strength coefficient K´ (MPa) are obtained from Fig. 3.5 and are shown in Table 3.6. Experimental values of n´ and K´ are verified by theoretical method as discussed in chapter 2 and shown in Table 3.7. It is observed that theoretical and expermintal values are in good agreement.

Table 3.7 Comparison of values of $n^{'}$ and $K^{'}$

parameters	experimental	theoretical
$n^{'}$	0.14322	0.142
$K^{'}$	545.7	541.2

Figure 3.9 illustrates variation of Vickers hardness and number of cycles of failure with respect to applied load. It is observed from Fig. 3.6 that as the number of cycles of failure reduced, so does the hardness value in LCF region.
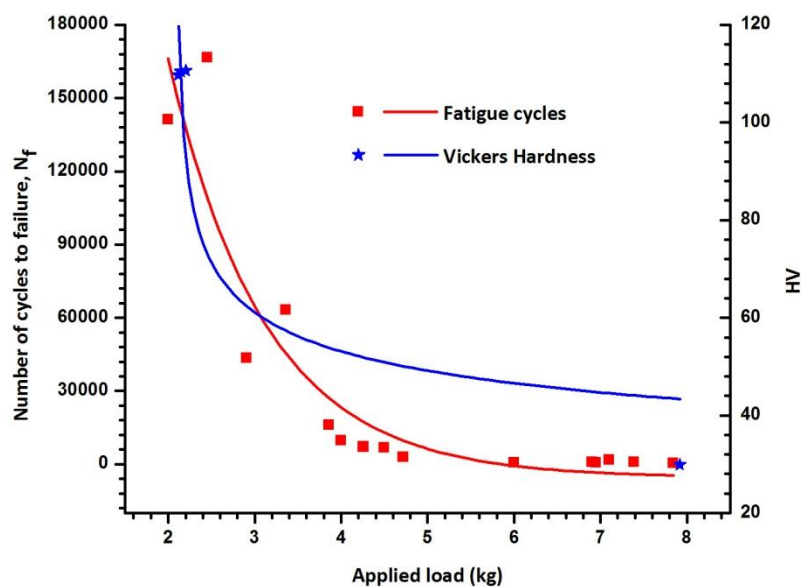

Fig. 3.6 Variation of Number of cycles of failure and Vickers hardness with applied force for as received AA6063 alloy

Table 3.8 demonstrates comparison of elastic and plastic strain obtained experimentally and numerically at a particular node on the surface of the specimen along the cross-section of failure. Differences of values obtained by two methods are negligible establishing the acceptability of results. It is also observed from Table 3.8 and Table 3.9 that empirical prediction for elastic strain is not good enough by SWT relation given by

Eq. (2.71) while that of plastic strain is satisfactory. Prediction for elastic and plastic strain by Morrows relation given by Eq. (2.72) is very good.

Table 3.8 Comparison of experimental, numerical and theoretical results for elastic strain as received AA6063 alloy

Force (N)	Cycles	Elastic Strain						
		Exp.	**FEM**	**% Diff.**	**SWT**	**% Diff.**	**Morrow**	**% Diff.**
140	133	0.00434	0.0045037	3.77	0.006124	41.109	0.005158	18.854

Table 3.9 Comparison of experimental, numerical and theoretical results for plastic strain AA6063 as received

Force (N)	Cycles	Plastic Strain						
		Exp.	**FEM**	**% Diff.**	**SWT**	**% Diff.**	**Morrow**	**% Diff.**
140	133	0.002077	0.019853	4.41	0.024222	16.622	0.020402	1.7711

Figure 3.10 illustrates variation of elastic and plastic strains over time at a particular node on the surface of the specimen along the fracture cross-section. It is observed from the figure that plastic strain is constant over time while elastic strain varies between maximum value of 0.00450368 and minimum value of 0.00309483.
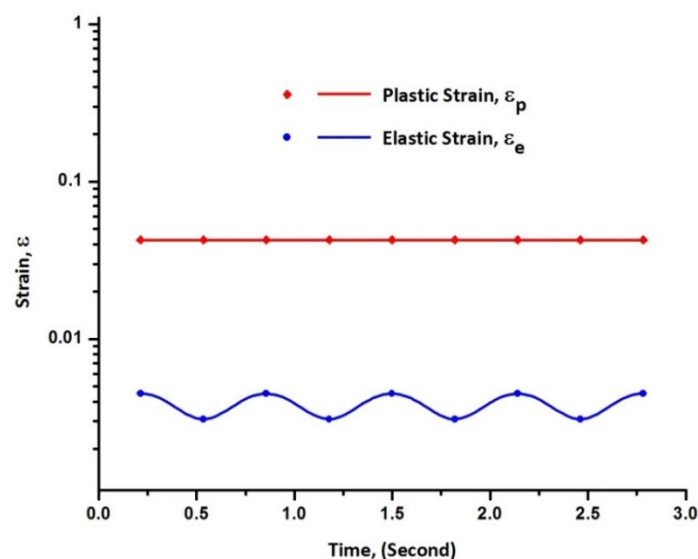
Fig. 3.7 Time history plot of elastic and plastic strain at surface node on cross section of fracture for as receivedAA6063-T6 alloy

Figures 3.11 and 3.12 show deformed shape of the specimen at a particular instant of time with elastic and plastic strain distributions, respectively.
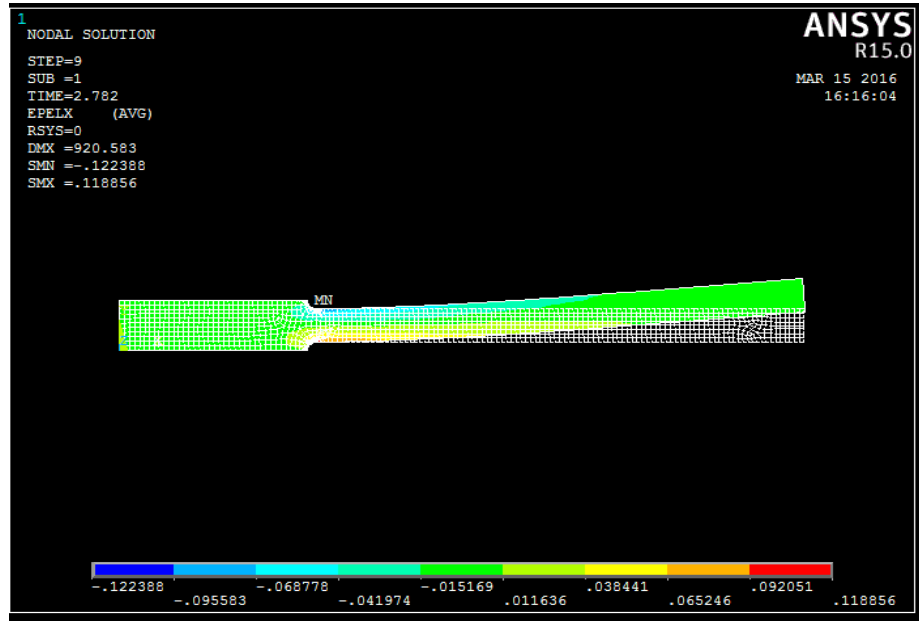

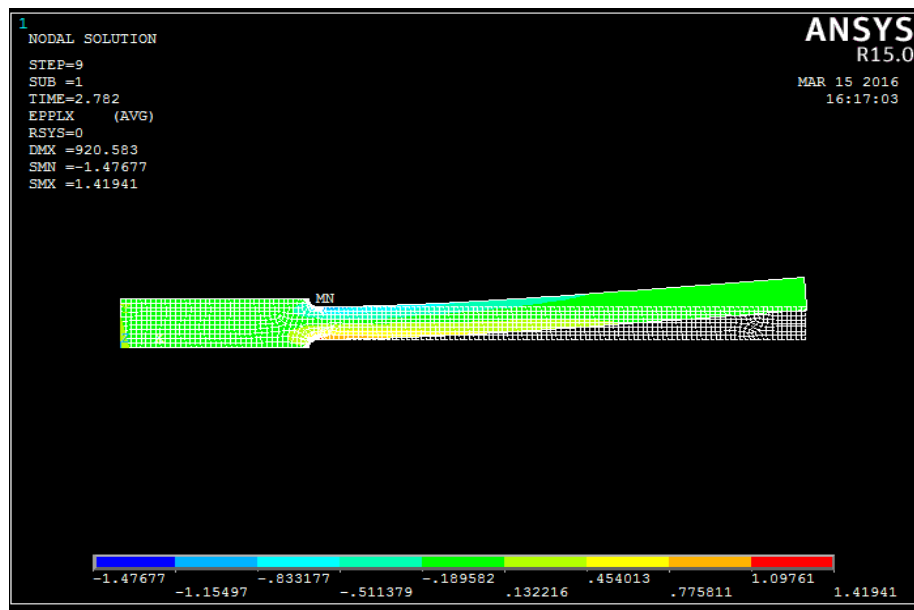**Fig. 3.8 Elastic strain at particular time on deformed shape for as received AA6063-T6 alloy**

Fig. 3.9 Plastic strain at particular time on deformed shape for as received AA6063-T6 alloy

Life Prediction of Low Cycle Fatigue Behavior of Rotating Cantilever Beam of aluminium alloy AA6063-T6 at Room Temperature

Chapter 3

Figure 3.13 demonstrates fitted lines for elastic strain-life data by experimental method, least square analysis, regression for model I and model II. Different lines show good fitting as points lie evenly above and below each line. Similarly Figs. 3.14 and 3.15 show fitting of plastic strain-life data experimental, least square, regression model I and model II. It can be observed from Figs. 3.13 to 3.15 that regression fit using model II in best closely fitting with that of experimental data. Moreover, plastic strain data and total strain data fitting are more closer than elastic strain data fitting using regression model II technique.
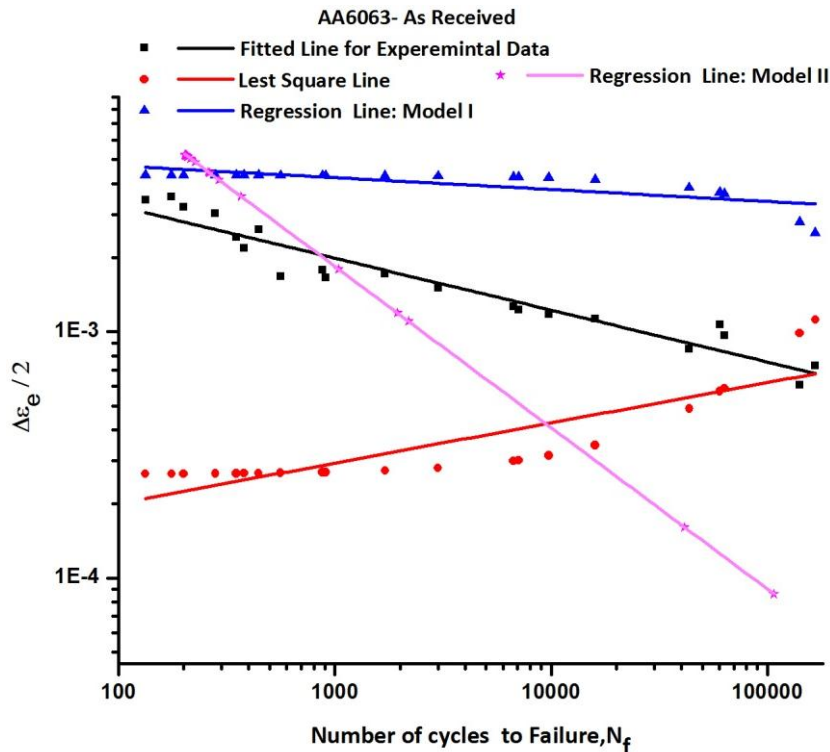

Fig. 3.10 Fitted elastic strain lines for as received AA6063 alloy

Table 3.10 shows values of R^2 and modified R^2 for elastic , plastic and total strain data. It is observed from this data that elastic, plastic and total strain are highly related linearly with number of cycles of failure.
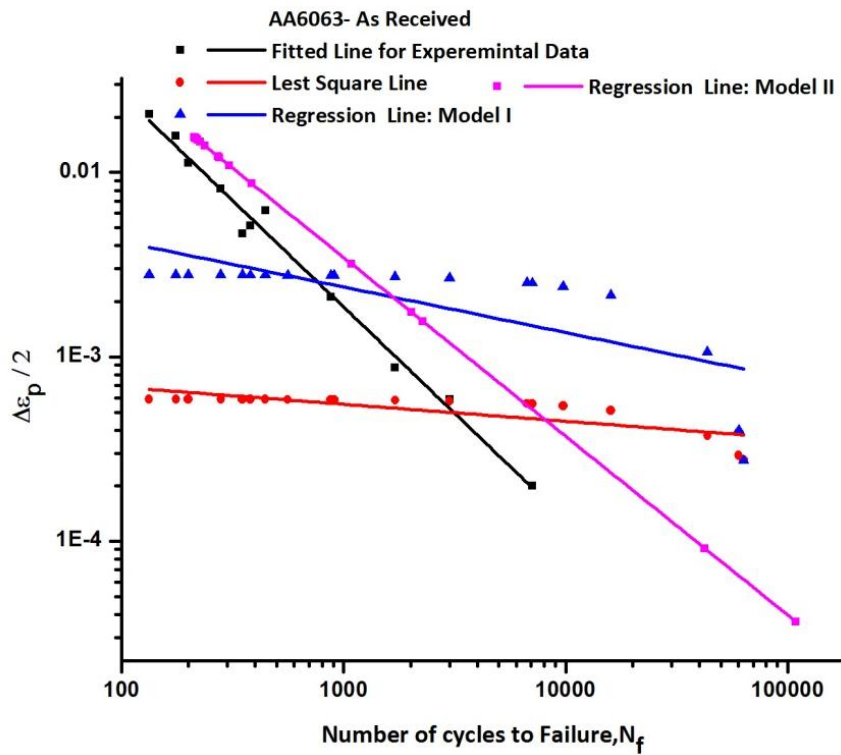
Life Prediction of Low Cycle Fatigue Behavior of Rotating Cantilever Beam of aluminium alloy AA6063-T6 at Room Temperature

Chapter 3

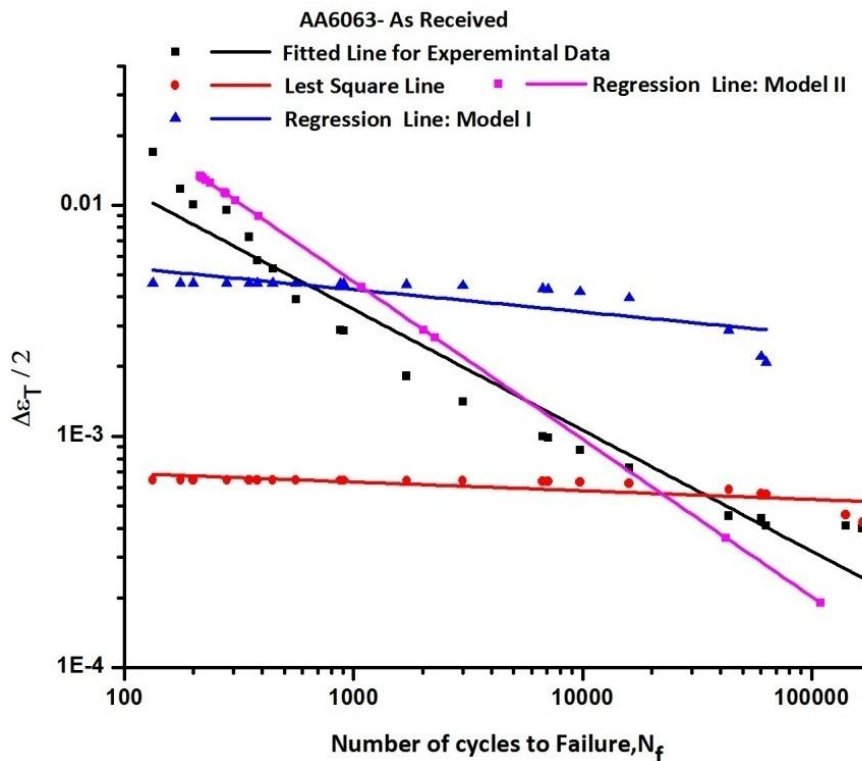**Fig. 11 Fitted plastic strain lines for as received AA6063 alloy**

Fig. 3.12 Fitted total strain lines for as received AA6063 alloy

Table 3.10 R^2 and modified R^2 values for elastic , plastic and total strain for as received AA6063-T6 alloy

Parameters	Elastic Strain	Plastic Strain	Total Strain
R^2	1.9722	0.14756	0.013728
Mod. R^2	-3.1871	-5.1078	-5.2487

Figure 3.16 explain how SWT parameter remain constant with number of cycles of failure for as received AA6063-T6 alloy rotating bending LCF data.
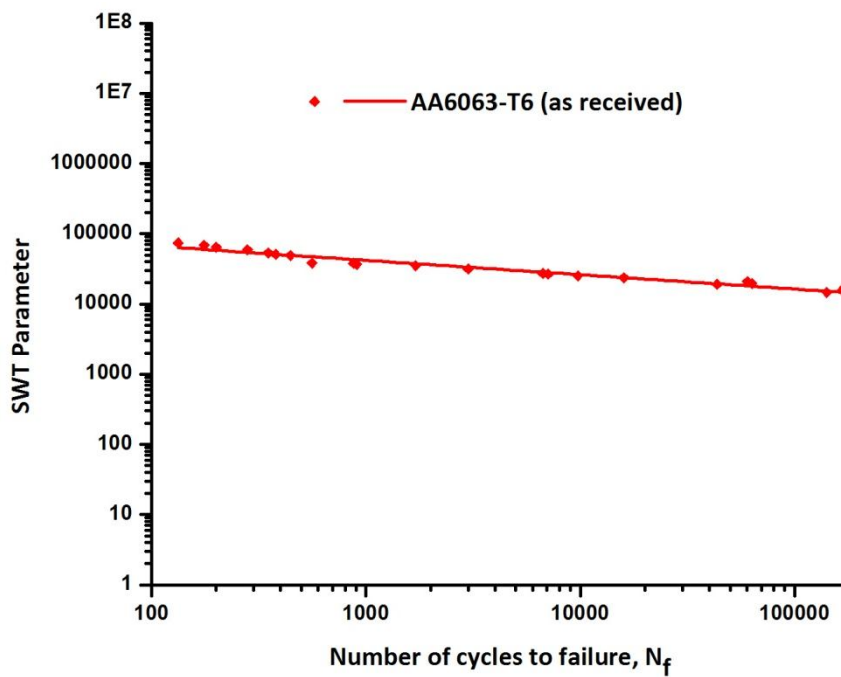

Fig. 3. 13 Variation of SWT parameter with number of cycles to failure

Life Prediction of Low Cycle Fatigue Behavior of Rotating Cantilever Beam of aluminium alloy AA6063-T6 at Room Temperature

Chapter 3

3.3 Conclusion

In the present chapter, low cycle fatigue behavior of as received AA6063-T6 at room temperature is investigated using rotating cantilever bending test. The fatigue parameters are calculated. These parameters are also obtained through theoretical approach and found to match with that obtained experimentally. Additionally tensile parameters also obtained from tensile test. Effect of variation of hardness on fatigue life is presented. The empirical analysis results are also presented.

The following conclusions are drawn from the investigation:

1. A good agreement is observed between experimental and theoretical values of LCF parameters, n' and K'.

2. It is also observed as the number of cycles of failure reduced ,so does the hardness value in LCF region.

3. From empirical analysis it is observed that elastic, plastic and total strain are highly linearly dependent on number of cycles of failure.

4. SWT parameter remain almost constant with number of cycle of failure.

5. SWT parameter provides good agreement to plastic strain while Morrow parameter provides good agreement to both elastic and plastic strain.

6. Experimental strain are in good agreement with numerical results.